

# Through-Space Ligand Interactions in Enantiomeric Dinuclear Ru Complexes

Nora Planas,<sup>[a]</sup> Gemma J. Christian,<sup>[a]</sup> Elena Mas-Marzá,<sup>[a]</sup> Xavier Sala,<sup>[a]</sup>  
Xavier Fontrodona,<sup>[b]</sup> Feliu Maseras,<sup>\*,[a, c]</sup> and Antoni Llobet<sup>\*,[a, c]</sup>

A family of dinuclear Ru complexes containing monodentate ligands displays dynamics based on supramolecular through-space interactions. The electronic and steric nature of the monodentate ligands allow a fine tuning of the kinetic parameters of this dynamic behavior that can be monitored by variable-temperature (VT) NMR spectroscopy.

Water oxidation to molecular dioxygen is a key reaction that needs to be fully understood in order to be able to design new energy-conversion schemes based on water and sunshine.<sup>[1]</sup> Furthermore, from a biological point of view it is an important reaction that takes place at the oxygen-evolving complex of PSII. However, even though it is under thorough scrutiny<sup>[2]</sup> its mechanisms are not fully understood. Hence the need to have low-molecular-weight functional models. While at the moment there are few well-defined complexes that have been shown to be capable of oxidizing water to molecular dioxygen even fewer of them have been studied from a mechanistic perspective.<sup>[3]</sup> Water nucleophilic attack to a high-valent Ru=O group and intramolecular O–O bond formation are the two metal-based mechanisms that have been observed so far based on experimental and theoretical grounds. While the synthetic demands for a catalyst capable of carrying out a nucleophilic water attack mechanism are relatively simple, for an intramolecular mechanism the catalysts are based on dinuclear complexes,

the structures of which are extraordinarily sophisticated. Thus it is imperative to understand all the relevant aspects of such a mechanism to be able to design efficient and robust water oxidation catalysts. In this particular field, the two key challenging factors that need to be addressed are first the degree of electronic coupling between the two metal centers through the bridging ligand and second the degree and nature of the through space interactions between the active groups that provides the right conditions so that an O–O bond can be formed. The present paper sheds light into the latter factor setting up the basis for further ligand/complex design.

We report here the synthesis and thorough characterization of a family of Ru–Hbpy (Hbpy = bis(2-pyridyl)pyrazole) related dinuclear Ru complexes (**1–9**, see Table 1) of general formula  $[\{\text{Ru}(\text{T})\}_2(\mu\text{-bpy})(\mu\text{-MeCOO})]^{n+}$  (T: 2,2':6',2''-terpyridine (trpy) or 1,3-bis(2-pyridylimino)isoin-dolinate ( $\text{bid}^-$ )) and  $[\{\text{Ru}(\text{T})(\text{L})\}_2(\mu\text{-bpy})]^{(n+1)+}$  (L = MeCN or substituted pyridines; see Figure 1 for the label assignment).

Table 1. Experimental and calculated free energies [in kcal mol<sup>-1</sup>] at 298 K, for the transition states of the isomeric interconversion reaction of complexes **1–9**, with general formula  $[\{\text{Ru}(\text{T})\}_2(\mu\text{-bpy})(\mu\text{-MeCOO})]^{n+}$  (T: trpy or  $\text{bid}^-$ ) and  $[\{\text{Ru}(\text{T})(\text{L})\}_2(\mu\text{-bpy})]^{(n+1)+}$  (L = H<sub>2</sub>O, MeCN, or substituted pyridines).

T	L	Complex	$\Delta G_{\text{expt}}^{\circ}$ (Solvent) <sup>[a]</sup>	$\Delta G_{\text{calcd}}^{\circ}$ (Solvent) <sup>[a]</sup>
$\text{bid}^-$	$\text{MeCOO}^{[b]}$	<b>1</b>	< 3.4 (D)	
$\text{bid}^-$	Py	<b>2</b>	7.2 (D)	7.76 (D)
$\text{bid}^-$	4-Me-py	<b>3</b>	8.5 (D)	9.29 (D)
$\text{bid}^-$	3,5-(Me) <sub>2</sub> -py	<b>4</b>	9.4 (D)	9.53 (D)
$\text{bid}^-$	4-CF <sub>3</sub> -py	<b>5</b>	9.5 (D)	9.06 (D)
$\text{bid}^-$	MeCN	<b>6</b>	10.4 (D)	14.3 (D)
trpy	$\text{MeCOO}^{[b]}$	<b>7</b>	< 4.2 (A)	
trpy	H <sub>2</sub> O	<b>8</b>	< 4.2 (A)	
trpy	Py	<b>9</b>	8.6 (A)	

[a] Solvents used are abbreviated as D for dichloromethane and A for acetone. [b]  $\text{MeCOO}^-$  acts as a bidentate bridging ligand between the two Ru metals and thus occupies the coordination positions of the two L ligands.

[a] N. Planas, Dr. G. J. Christian, Dr. E. Mas-Marzá, Dr. X. Sala,  
Prof. F. Maseras, Prof. A. Llobet  
Institute of Chemical Research of Catalonia (ICIQ)  
Av. Països Catalans 16, 43007 Tarragona (Spain)  
Fax: (+34) 977-920-228  
E-mail: allobet@iciq.es

[b] Dr. X. Fontrodona  
Serveis Tècnics, Universitat de Girona  
Campus de Montilivi, 17071 Girona (Spain)

[c] Prof. F. Maseras, Prof. A. Llobet  
Departament de Química  
Universitat Autònoma de Barcelona  
Cerdanyola del Vallès, 08193 Barcelona (Spain)

Supporting information for this article is available on the WWW under <http://dx.doi.org/10.1002/chem.201000585>.

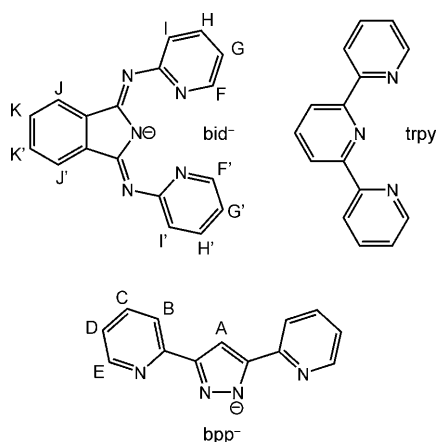


Figure 1. Drawing of the ligands and labeling used for the  $^1\text{H}$  NMR assignment.

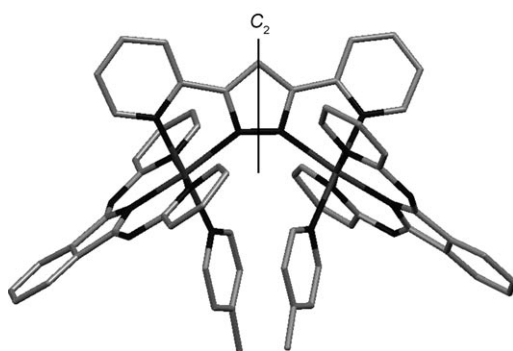


Figure 2. X-ray crystal structure of the cationic part of  $\Delta,\Delta$ -**3**. The  $C_2$  axis is shown with a broken line. The  $\text{bpp}^-$  ligand is placed in the plane of the paper, whereas the meridional  $\text{bid}^-$  ligands are nearly perpendicular to the mentioned plane. Dark gray: Ru; black: N; light gray: C. H atoms have been omitted for clarity.

This family of complexes constitutes an ideal basis to understand and quantify ligand through-space interactions.

Figure 2 shows the cationic moiety the complex  $\Delta,\Delta$ -**3**,<sup>[4]</sup> containing 4-picoline ligands.

These molecules possess  $C_2$  symmetry with the  $C_2$  axis running through the pyrazolate group, bisecting the N–N bond and through to the opposite C atom of the pyrazolate ring. As it can be observed in Figure 2, each metal center has a distorted octahedral geometry, due to both the bite angle of the chelating ligands and to the need to accommodate the encumbering monodentate ligands.

The distortion can be described as an inverse synchronized rotation of the pyridyl  $\text{bpp}^-$  groups (the angle between these two pyridyls is  $17.5^\circ$ ) from an ideal octahedral geometry through an imaginary axis that would go through the C–C bonds connecting the pyridyl and pyrazolate groups of the  $\text{bpp}^-$  ligand. This distortion provokes the displacement of the metal center above and below the equatorial plane in which the  $\text{bpp}^-$  ligand would normally lie.

It is also interesting to observe that the rings of the monodentate picoline ligands lie nearly parallel to one another (angle between best planes is  $3.2^\circ$ ) and with the distance between the centroids of the pyridine rings of  $3.43 \text{ \AA}$  suggesting significant  $\pi$ – $\pi$  interactions.

In solution at room temperature the two enantiomers shown in Figure 3 rapidly interconvert between each other. As a consequence the resonances observed in the NMR spectrum at RT can be interpreted as if the molecule possessed  $C_{2v}$  symmetry for the case of **1**. For the case of the other complexes with N-containing monodentate ligands, some of the resonances at RT are so wide that they are nearly not observed. Variable-temperature (VT) NMR spectroscopy (298–218 K) makes it possible to monitor the speed of this equilibrium as shown in Figure 4 for the pair of enantiomers  $\Delta,\Delta$ -**4** and  $\Lambda,\Lambda$ -**4**, and thus the activation energy can be extracted for this isomeric interconversion process. No evidence in the NMR spectra is observed for Ru–N bond breaking under these conditions, indicating that the interconversion involves ligand-rotation processes only, besides

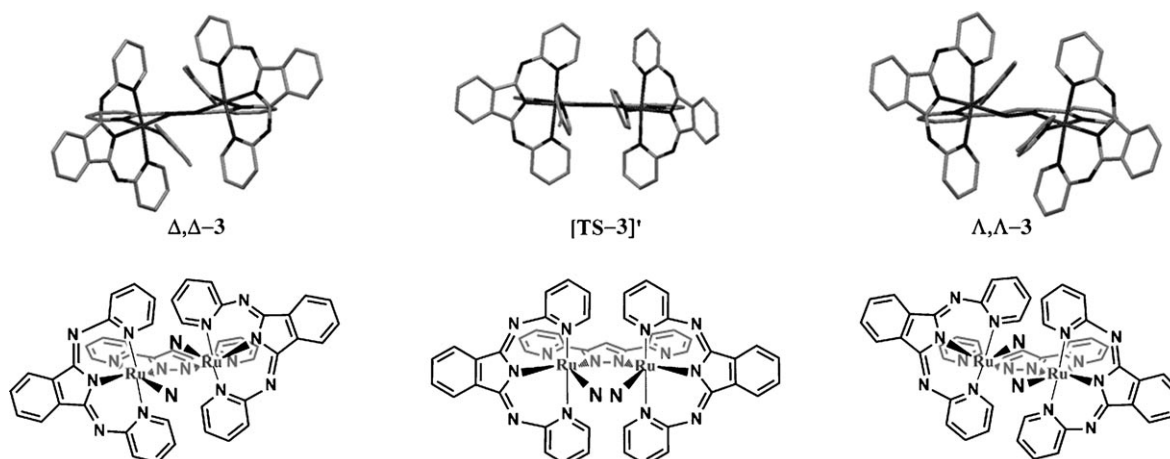


Figure 3. Top: Stick models for the cationic parts of **3**. Left: X-ray crystal structure of  $\Delta,\Delta$ -**3**. Center: Computed transition-state structure of  $[\text{TS-3}]'$ . Right: Computed structure of  $\Lambda,\Lambda$ -**3**. In all cases the  $\text{bpp}^-$  ligand is placed perpendicular to the plane of the paper. Bottom: ChemDraw drawings of the top structures. The monodentate 4-picoline ligand is not drawn for clarity and is represented by bold-typeface Ns.

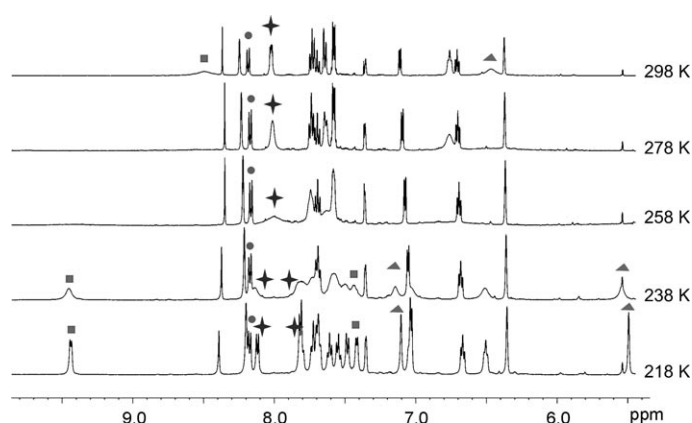


Figure 4. VT  $^1\text{H}$  NMR spectra of **4** in  $\text{CD}_2\text{Cl}_2$ . The assignment of the resonances is keyed in Figure 1. The different symbols indicate the splitting observed upon reducing the temperature: squares are for  $\text{H}_\text{F}$  and  $\text{H}_\text{F}'$ , spheres for  $\text{H}_\text{E}$ ; stars for  $\text{H}_\text{J}$  and  $\text{H}_\text{J}'$ ; and triangles for  $\text{H}_\text{L}$  (*ortho*-protons of the 3,5-lutidine ligand).

the correspondingly coupled vibrations, translations, and solvent interactions.

DFT/MM calculations<sup>[5]</sup> have been used to study the reaction pathway for the interconversion process. The enantiomers are found to be connected through the transition state shown in Figure 3 (center), which has an approximately planar  $\text{bpp}^-$  backbone with the metal centers lying in the plane defined by the ligand. The picoline ligands remain parallel to one another (angle between planes is  $3.8^\circ$ ) and approximately perpendicular to the equatorial plane. However, unlike the enantiomers they are almost eclipsed, forcing the methyl substituents closer together. It is likely for this reason that the distance between the centroids of the picoline rings in the transition state is larger ( $3.71 \text{ \AA}$ ) compared to the two enantiomers. The increase in strain in the rest of the molecule results in longer  $\text{Ru-N}(\text{bpp}^-)$  bond lengths and a more open  $\text{N}(\text{pyrazol-bpp}^-)\text{-Ru-N}(\text{picoline})$  bond angle.

The transition vector is associated both with flexing of the backbone  $\text{bpp}^-$  ligand and with the rotation of the  $\text{Ru-N}(\text{picoline})$  bonds with respect to each other. Clockwise rotation of the axes defined by the  $\text{Ru-N}(\text{picoline})$  bonds and corresponding flexing of the  $\text{bpp}^-$  ligand generates the  $\Delta, \Delta$  isomer, while anticlockwise rotation generates the  $\Lambda, \Lambda$  isomer [Eq. (1)].



While in this case both movements have an important contribution to the transition vector, it is likely that for related ligand systems with more rigid meridional ligands, the transition vector may have a larger contribution from the rotation of the  $\text{Ru-N}$  axes than from backbone ligand movement.

Table 1 presents the experimental<sup>[7]</sup> and DFT-calculated activation barriers obtained for the family of complexes **1–9**. In general the calculated activation barriers slightly overesti-

mate the experimental values, but reproduce the experimental trends. From the table the activation barriers are found to vary depending on the class of monodentate ligand, with higher activation barriers observed for the nitrile ligand, which is known to have stronger  $\pi$ -backbonding interactions,<sup>[6]</sup> than for the pyridylic type of ligands (compare complexes **2** and **6** in Table 1). In comparison, the lowest activation barriers were found for the O-donor ligands (compare **1**, **7**, and **8** with **2**). The activation barriers were also found to be dependent on the meridional ligand where lower activation barriers were found for the more flexible  $\text{bid}^-$  ligand than for the  $\text{trpy}$  ligand. Finally, within the family of pyridylic ligands, the activation barriers increase with steric bulk, from  $\text{L} = \text{pyridine}$ ,  $\text{picoline}$ , to  $\text{lutidine}$ .

The trends in activation barriers can be rationalized by considering the nature of the transition state in which the  $\text{Ru-N}(\text{picoline})$ , or more generally  $\text{Ru-N}(\text{L})$ , axes are approximately eclipsed. For the pyridylic type ligands, the substituents of the pyridine ring are forced closer together, leading to increasing activation barriers as the number of substituents increases. The increasing steric strain can be seen in the distance between the centroids of the pyridylic rings, which increases from  $3.69$ , to  $3.71$  to  $3.78 \text{ \AA}$ , for pyridine, picoline, and lutidine, respectively. The differences in activation energies between types of ligand donors can also be attributed to through-space interactions and the rearrangement required to reach the transition state. This is most significant for the  $\text{MeCN}$  ligand, for which the rearrangement required to reach the transition state is greatest, and consequently gives the highest barrier. The O-donor ligands, however, either bridge the metal centers,  $\text{MeCOO}^-$ , or have little steric bulk,  $\text{H}_2\text{O}$ , so the rearrangement required and steric strain in the transition state is not as significant, resulting in much lower activation barriers.

This family of complexes, therefore, provides a basis to understand the electronic and steric factors that influence the interconversion process and thus the dynamics involved in Equation (1). These are shown to be chiefly governed by the monodentate ligands for which the degree of through-space interactions (an intra-supramolecular effect) dictates the interconversion barriers. Furthermore the design of the complex is fundamental. In particular the bridging  $\text{bpp}^-$  ligand, which acts as backbone for the two metal centers, places them at the correct distance and relative orientation to allow this dynamic behavior. At longer distances the through-space interactions would be too weak and the metal centers would acquire an ideal type of octahedral geometry and no dynamic effects would be observed. In contrast if the two monodentate ligands were placed too close the barriers would be so high that at RT the isomeric interconversion would not occur. Thus, the present family of complexes display the delicate electronic and steric balance needed for these intra-supramolecular interactions to take place. In turn, this understanding is of paramount importance in order to design water oxidation catalysts, especially for the particular case in which the oxygen–oxygen bond formation takes place in an intramolecular manner. Thus, in cases in

which the monodentate ligand is an aqua ligand, the access to higher oxidation states provides Ru=O groups properly oriented and with the right through-space interaction that, once generated, are ready to couple to one another and thus provide a viable scenario for the elusive intramolecular mechanism.

We have prepared and thoroughly characterized a family of dinuclear Ru complexes in which the through-space interaction can be fine-tuned by steric and electronic effects. In particular we have shown that the  $\text{bpp}^-$  pyrazolate bridge acts as a spectator ligand, but also provides the right topology so that the monodentate ligands bonded to them can adequately interact in a supramolecular manner. We have also put forward the important implication this control has for the future design of water oxidation catalysts. Finally, this work constitutes an unprecedented example in which the dynamic behavior between two ligands bonded to two different metals is established and understood.<sup>[8]</sup>

### Acknowledgements

Support from SOLAR-H2 (EU 212508), ACS (PRF 46819-AC3), MEC (CTQ2007-67918 and CTQ2008-06866-CO2-02) and from the Consolider Ingenio 2010 (CSD2006-0003) are gratefully acknowledged.

**Keywords:** N ligands • NMR spectroscopy • ruthenium • structure elucidation

- [1] See, for instance: X. Sala, M. Rodríguez, I. Romero, L. Escriche, A. Llobet, *Angew. Chem.* **2009**, *121*, 2882; *Angew. Chem. Int. Ed.* **2009**, *48*, 2842.
- [2] a) J. Yano, J. Kern, K. Sauer, M. J. Latimer, Y. Pushkar, J. Biesiadka, B. Loll, W. Saenger, J. Messinger, A. Zouni, V. K. Yachandra, *Science* **2006**, *314*, 821; b) M. Haumann, P. Liebisch, C. Müller, M. Barra, M. Gräbner, H. Dau, *Science* **2005**, *310*, 1019.
- [3] a) J. J. Concepcion, J. W. Jurss, J. L. Templeton, T. J. Meyer, *J. Am. Chem. Soc.* **2008**, *130*, 16462; b) S. Romain, F. Bozoglian, X. Sala, A. Llobet, *J. Am. Chem. Soc.* **2009**, *131*, 2768; c) F. Liu, J. J. Concepcion, J. W. Jurss, T. Cardolaccia, J. L. Templeton, T. J. Meyer, *Inorg. Chem.* **2008**, *47*, 1727; d) J. J. Concepcion, J. W. Jurss, J. L. Templeton, T. J. Meyer, *Proc. Natl. Acad. Sci. USA* **2008**, *105*, 17632; e) F. Bozoglian, S. Romain, M. Z. Ertem, T. K. Todorova, C. Sens, J. Mola, M. Rodríguez, I. Romero, J. Benet-Buchholz, X. Fontrodona, C. J. Cramer, L. Gagliardi, A. Llobet, *J. Am. Chem. Soc.* **2009**, *131*, 15176–15187; f) S. Romain, L. Vigara, A. Llobet, *Acc. Chem. Res.* **2009**, *42*, 1944.
- [4] For these complexes the helicity and the connectivity are exactly the same for both enantiomers and, the chirality arises from the different orientations of the monodentate ligand, either above or below the equatorial plane defined by the  $\text{bpp}^-$  ligand. Therefore, the assignment has been carried out in an arbitrary manner.
- [5] ONIOM(B3LYP:UFF) calculations with solvent and free-energy corrections. See the Supporting Information for computational details.
- [6] C. Sens, M. Rodríguez, I. Romero, A. Llobet, T. Parella, J. Benet-Buchholz, *Inorg. Chem.* **2003**, *42*, 8385.
- [7] H. Friebolin in *Basic One- and Two-Dimensional NMR Spectroscopy*, 4th ed., Wiley-VCH, Weinheim, **2004**, pp. 158–370.
- [8] G. R. Owen, J. Stahl, F. Hampel, J. A. Gladysz, *Chem. Eur. J.* **2008**, *14*, 73.

Received: March 5, 2010  
Published online: June 8, 2010